PCCP

Accepted Manuscript

This is an *Accepted Manuscript*, which has been through the Royal Society of Chemistry peer review process and has been accepted for publication.

Accepted Manuscripts are published online shortly after acceptance, before technical editing, formatting and proof reading. Using this free service, authors can make their results available to the community, in citable form, before we publish the edited article. We will replace this *Accepted Manuscript* with the edited and formatted *Advance Article* as soon as it is available.

You can find more information about *Accepted Manuscripts* in the **Information for Authors**.

Please note that technical editing may introduce minor changes to the text and/or graphics, which may alter content. The journal's standard **Terms & Conditions** and the **Ethical guidelines** still apply. In no event shall the Royal Society of Chemistry be held responsible for any errors or omissions in this *Accepted Manuscript* or any consequences arising from the use of any information it contains.

Chemical Science

ARTICLE

A Biomimetic Molecular Switch at Work: Coupling Photoisomerization Dynamics to Peptide Structural Rearrangement

Cristina García-Iriepa,[a,b] Moussa Gueye,[c] Jérémie Léonard,*[c] David Martínez-López,[a] Pedro J. Campos,[a] Luis Manuel Frutos,[b] Diego Sampedro*[a] and Marco Marazzi*[d†]

In spite of a considerable interest in the design of molecular switches towards photo-controllable (bio)materials, few studies focused on the major influence of the surrounding environment on the switches photoreactivities. We present a combined experimental and computational study of a retinal-like molecular switch linked to a peptide, elucidating the effects on the photoreactivity and on the α-helix secondary structure. Temperature-dependent, femtosecond UV-Vis transient absorption spectroscopy and high-level hybrid quantum mechanics/molecular mechanics methods were applied to describe the photoisomerization process and the subsequent peptide rearrangement. It was found that the conformational heterogeneity of the ground state peptide controls the excited state potential energy surface and the thermally-activated population decay. Still, a reversible α-helix to α-hairpin conformational change is predicted, paving the way for a fine photocontrol of different secondary structure elements, hence (bio)molecular functions, using retinal-inspired molecular switches.

Introduction

Molecular machines, such as switches and motors, are becoming essential components for biochemistry and materials science.[1, 2] This prompts the synthesis and characterization of a great variety of derivatives to tailor their properties for specific applications. Among them, molecular switches (especially when photoactive) are the most studied devices due to their simple mechanism and immense applications.[3]

Therefore, the photophysics and photochemistry of the most known photoactive molecular switches have been extensively investigated,[4] and their efficient application and inclusion into real systems is the next step, which is now an emerging and challenging task. One of the most important fields where photoswitches are being applied is biochemistry, in terms of photomodulation of biological properties.[5-7] Azobenzenes is the largest family of

switches used for the control of biomolecules. They have been incorporated into nucleic acids, receptors, channels, peptides, etc.[8-10] Stilbenes,[11-13] hemithioindigos[14, 15] and the retinal protonated Schiff base (PSB) derived chromophores[16-18] have been used in similar applications but to a lower extent.

The ability of molecular photoswitches to control the structure by using a convenient external stimulus allows to envisage fascinating applications in which the function of complex systems could be easily turned on and off. Attractive targets for this approach are proteins and peptides. In these compounds, the function and the structure are strongly linked and they mediate in a huge number of biological relevant processes. From enzymatic catalysis to ligand recognition, proteins are involved in diverse physiological actions.[19] Also, a good number of diseases (Parkinson's and Alzheimer's diseases, among others) are linked to structural changes in proteins.[20, 21] In this regard, different model peptides cross-linked with azobenzene have been studied by circular dichroism or IR spectroscopies together with molecular dynamics (MD) simulations to understand the peptide conformational change after photoisomerization.[22-27] Recently, the first example of a retinal-like switch linked to a peptide has been reported. The photoisomerization of the switch causes a large change in its end-to-end distance, which in turn modifies the peptide secondary structure.[17] The advantages of this type of switches for that application are their high photoisomerization quantum yield,[17, 28] photostability[29] and large end-to-end distance change.[17]

Using this approach, it could be possible to modify to a great extent the secondary structure (and consequently the function) of any given peptide or protein. While the α-helix is the most

[a.] Departamento de Química, Centro de Investigación en Síntesis Química (CISQ), Universidad de La Rioja, Madre de Dios 53, E-26006 Logroño, Spain.
E-mail: diego.sampedro@unirioja.es
[b.] Unidad Docente de Química Física, Universidad de Alcalá, E-28871 Alcalá de Henares, Madrid, Spain
[c.] Institut de Physique et Chimie des Matériaux de Strasbourg & Labex NIE, Université de Strasbourg, CNRS UMR 7504, 23 rue du Loess, Strasbourg 67034, France.
E-mail : leonard@ipcms.u-strasbg.fr
[d.] Department of Theoretical Chemical Biology, Institute of Physical Chemistry, KIT, Kaiserstrasse 12, 76131 Karlsruhe, Germany.
E-mail: marco.marazzi@univ-lorraine.fr

abundant structure in proteins, its formation is strongly dependent on the number and type of aminoacids, the solvent and the presence of ions in solution. From the Zimm–Bragg model[30] to the work of Baldwin *et al.*[31-33] many efforts have been made in the last decades to learn how the proteins achieve their secondary structure both from the theoretical and experimental points of view. In those studies, the content of α-helix is determined by the intrinsic properties of the proteins (sequence of amino acids). Alternatively, this helicity could be also altered by an external stimulus such as light. For instance, the dynamics of helix formation was studied after photolysis of disulfide bridges.[34,35] However, while this contributes to a deeper understanding of the folding process, it lacks the ability to control it.

Moreover, few studies focus on how the photochemistry of the switch itself is affected upon linkage to the peptide. Yet this is a very fundamental question towards effective molecular function switching, especially when using PSBs, since the linkage of the switch may strongly affect its photoreactivity, as exemplified *e.g.* by the very different photoreaction of retinal in rhodopsins as compared to homogeneous solvent.[36-40]

Here, we report on a combined experimental and computational study of the photoisomerization dynamics of a protonated retinal-like molecular switch covalently linked to a recently reported[17] α-helical peptide. We disclose a detailed comparative study of the molecular switch photochemistry linked to the peptide with respect to a homogeneous solvent environment. Moreover, we analyze the structural modification of the cross-linked peptide from an α-helix to an α-hairpin upon photoisomerization. The model system is illustrated in Figure 1.
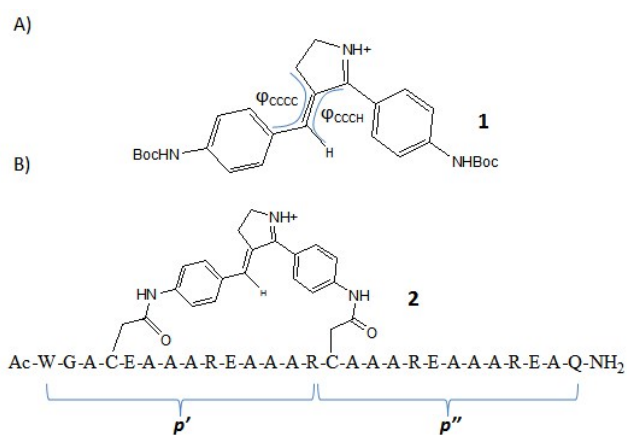

Figure 1. A) Structure of compound *E*-1, studied in MeOH. The dihedral angles ϕ_{CCCC} and ϕ_{CCCH} are introduced to describe the photoreactive motion of the switch. B) Compound *E*-2, studied in water. The switch is linked to the cysteine residues of the peptide. The two halves of the peptide are labeled *p'* and *p''* as illustrated.

The *tert*-butyloxycarbonyl (BOC) protected (*E*)-4-(4-(4-aminobenzylidene)-3,4-dihydro-2*H*-pyrrol-5-yl)aniline is the molecular photoswitch investigated both in solution, compound *E*-1, or linked to the peptide, forming compound **2**. The peptide is a Marqusee and Baldwin type of peptide, with a high content of alanine residues favoring an α-helical structure.[31, 32] By implementing UV-Vis transient absorption spectroscopy, MD and

hybrid quantum mechanics/ molecular mechanics (QM/MM) methods, we show that the photoisomerization occurs through a conical intersection after thermal activation over an excited-state (S_1) potential energy barrier for both compounds, with very similar time-resolved spectral signatures. While the S_1 decay kinetics is monoexponential for compound **1** (*i.e.* homogeneous solvent environment), it appears multiexponential for compound **2**, due to the structural heterogeneity of the cross-linked peptide. We conclude that the main influence of the peptide linkage on the photoreactivity of the switch is to increase the S_1 energy barrier to a magnitude that depends on the ground state (S_0) conformation of the cross-linked peptide. We are able to rationalize the effect of the peptide linkage on the switch photoisomerization, and propose the underlying mechanism, including the subsequent effect on the peptide conformation.

Methods

Experimental Techniques. Compounds **1** and **2** were synthesized and purified as previously reported.[17] Transient absorption spectroscopy (TAS) is performed with a 400-nm pump pulse, and reveals the time evolution of the pump-induced absorption changes in the UV-VIS spectral range, with a 70-fs time resolution, at temperatures of 10°C, 24°C and 50°C. The experimental set-up and data analysis by global fitting (assuming multiexponential kinetics) have been described previously[41] and are briefly recalled in the ESI.

Computational Strategy. A multi-scaling approach was adopted, considering the different tasks to be performed: classical MD was employed for the peptide conformational study, while hybrid QM/MM methods were applied to calculate photophysical and photochemical properties related to electronic absorption and photoswitching mechanism.

Peptide conformations were evaluated by MD simulations (10 MD simulations of 50 ns (100 ns for *Z*-2)) where the peptide was represented by the AMBER99SB force field[42] and the molecular switch by the generalized AMBER force field (GAFF,[43] see details in the ESI).

The electronic vertical transitions were calculated for the optimized *E*-1 and 50 MD snapshots of *E*-2 and *Z*-2 at the (TD-)DFT/MM level of theory, calibrated with MS-CASPT2//SA-2-CASSCF/MM level of theory.[44] In all models, the photoswitch was included in the QM region, resulting in an active space of 12 electrons in 12 orbitals. *E*-to-*Z* minimum energy paths (MEPs) were calculated on S_1 at the SA-2-CASSCF level of theory and single point MS-CASPT2 corrections were performed along them to quantitatively determine vibrational excess energies and excited state energy barriers. Moreover, on-the-fly non-adiabatic molecular dynamics were computed[45] at the CASSCF/MM level from the Franck–Condon point and from the S_1 transition state (see ESI for the details).

All MD trajectories were simulated with Gromacs 4.6;[46] MM parameters for the photoswitch were generated by the Antechamber program as part of AmberTools14.[47] MS-CASPT2//SA-2-CASSCF/MM calculations were performed with the Molcas 8 program[48] interfaced to Tinker 6.3.2,[49] TD-DFT/MM calculations were run with the M062X functional[50] through the Gaussian

09[51]/Tinker 4.2 interface, while MP2/MM calculations were performed with the Gaussian 09 ONIOM method.[52] The 6-31G(d) basis set was employed in all CASSCF and CASPT2 calculations, while the 6-311+G(d,p) basis was used for TD-DFT calculations.

Experimental Results

When freshly dissolved in MeOH in the dark at room temperature, compound **1** is in the pure *E* isomer form (**E-1**).[17] The *Z* isomer may be accumulated by illumination at 400 nm. Figure 2A displays the steady state absorption spectra of the dark and illuminated samples in acidic (pH = 4.3) MeOH solution. (pH = 4.3) MeOH solution. A buffer solution was used in all the experiments to ensure the protonated nature of the retinal-like switches. This allows for the use of visible light to activate the switch, as we have previously described.[17] The UV-Vis steady state absorption of the **E-2** in 2-(*N*-morpholino) ethanesulfonic acid (MES) buffer solution at pH = 4.3 is displayed in Figure 2B. Irradiating the **E-2** solution at 400 nm yields a photo-stationary state (PSS) which was reported to be a 93/7 *Z/E* isomer mixture.[17]
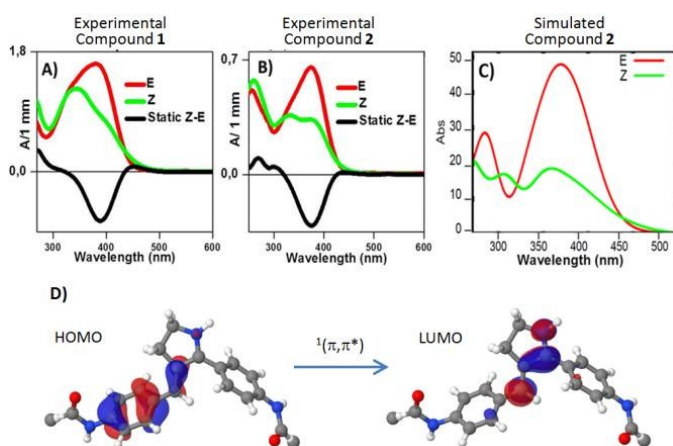

Figure 2. Absorption spectra of (A) the **E-1** (red line) and **Z-1** (green line) in acidic MeOH and (B) the **E-2** (red line) and **Z-2** (green line) in buffer solution at pH= 4.3. The *Z-E* difference spectra (black curves) are useful for the interpretation of transient absorption data below. C) Simulated absorption spectra of the protonated **E-2** and **Z-2** in water at the TD-DFT/MM level of theory. D) Molecular orbitals involved in the $S_0 \rightarrow S_1$ electronic transition, showing the charge transfer character along the backbone.

Figure 3 compares the transient absorption changes (*i.e.* differential absorption ΔA) of compounds **E-1** and **E-2** in acidic conditions after excitation at 400 nm at 24°C (see experimental details in the ESI). In the ΔA 2D-maps (Figure 3 A, F) negative ΔA, coded in blue, is due to the ground state bleach (GSB) or stimulated emission (SE), while positive, red-coded ΔA represents excited-state absorption (ESA) or photoproduct absorption (PA) bands. Both compounds display similar TAS spectral signatures dominated by several 10- to 100-ps- long-lived GSB at wavelengths < 410 nm, ESA from ~415 nm to ~500 nm, and SE from ~500 nm to > 600 nm. Noticeably, at very early times the ESA signatures appear red-

shifted, especially in **E-2** where it is seen to extend until > 600 nm and where the initial negative signal around 440 nm is attributed to an initially blue-shifted stimulated emission (see the spectrum at 50 fs in Figure 3G). Fast spectral relaxation characterized by the concomitant blue shift of the ESA and/or red shift of the SE occurs on the 100-fs time scale in both molecules, although it is more pronounced in **E-2** (see Figures 3B, G). This is indicative of reactive motion out of the Franck–Condon (FC) region on this time scale. Further rise or red-shift of the SE band occurs within several ps in both compounds and is accompanied by the ESA blue shift on the same time scale in the case of **E-2**. This may be attributed to further structural molecular and (polar) solvent relaxation and thermalization in S_1. Subsequently, all TA signatures decay with no further change in the spectral shapes within a few 10 ps for **E-1** and a few 100 ps for **E-2** (Figures 3C, H), indicative of the decay to the ground state (S_0) on these time scales. After complete spectral relaxation over the ns time scale, a quasistatic spectrum is observed for both compounds (see Figures 3D, I), which overlaps perfectly with the *Z-E* steady state difference spectra, evidencing the formation of the *Z* isomer in both cases. Possibly, the *Z* isomers are formed earlier, presumably upon decay to S_0, but their final thermally-relaxed forms characterized by the steady-state difference spectra are observed only after complete vibrational relaxation and thermalization.
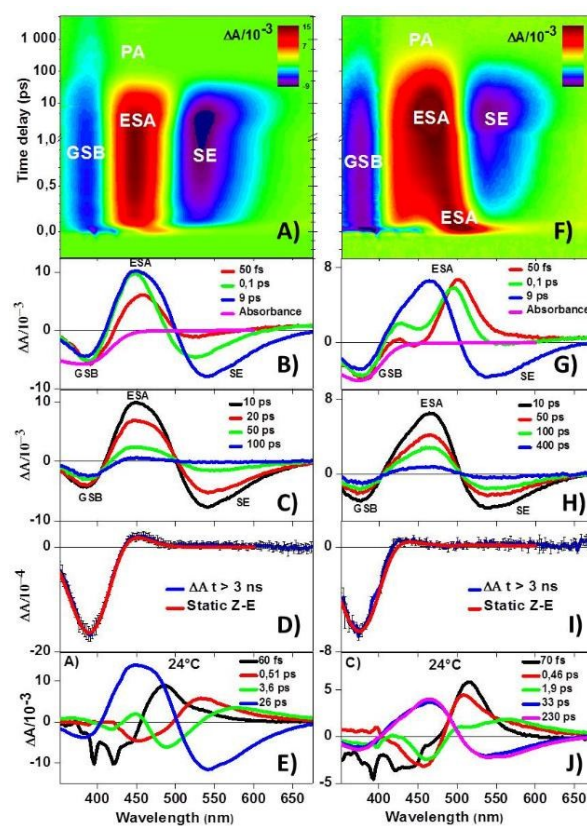

Figure 3. A, F) Room-temperature (24°C) 2D transient absorption data (ΔA in color code) as a function of wavelength (nm) and pump-probe time delay (ps) for the dark-adapted solutions of **E-1** in acidic MeOH and **E-2** in aqueous buffer solution at pH= 4.3, respectively. B, G) Transient spectra at early time delays (S_1 relaxation kinetics):

the magenta curves are the opposite of the steady-state absorbance, proportional to the pure GSB signature. C, H) Transient spectra at intermediate time delays (S_1 decay). D, I) Quasi-static spectra obtained at a time delay > 3 ns (blue) overlapped with the *Z-E* steady-state difference spectra (red). E, J) Decay-Associated Spectra (DAS) obtained by global analysis of the 24°C TAS data.

When changing the temperature from 24°C to 10°C or 50°C, similar TAS signals are observed, but kinetics time scales change. The results of the global analysis (see ESI) are disclosed in the form of decay-associated spectra (DAS) displayed in Figure 3E and 3J for both compounds at 24°C and in Figure S1 (see ESI) at 10°C and 50°C. Table 1 summarizes all time constants revealed by the global analysis for both compounds, as a function of temperature.

For both compounds at any temperature, the DAS corresponding to the shortest 3 time constants (black, red and green curves in Figure 3E, J) have dispersive-like shapes with negative amplitudes at shorter wavelengths and positive amplitudes at longer wavelengths. These are the signatures of the dynamic spectral shift discussed above (Figure 3B, F) caused by excited state vibrational relaxation and solvation, which most likely obeys non-exponential dynamics. The present data analysis, however, postulates multiexponential decay kinetics, and therefore yields 3 time constants which should be considered as typical time scales over which such non-exponential dynamics and corresponding spectral shifts occur in S_1. The fastest of these times constants, τ_1, in the range of 60 to 90 fs (*i.e.* close to the experimental time resolution and therefore uncertain, possibly shorter) is essentially the same for both compounds and temperature-independent (see Table 1). It is attributed to the early reactive motion, along high frequency modes, out of the Franck–Condon region. Such motion is triggered by the initial slope of the (displaced) S_1 PES, and possibly releases a vibrational energy much larger than thermal energy, as confirmed by the minimum energy path computations below.

The next two time constants τ_2 and τ_3 in the range of 0.2 to 4 ps are attributed to further vibrational relaxation involving lower-frequency modes, towards the minimum of the S_1 potential surface (PES) and possibly also solvent equilibration on the few ps time scale. While they are temperature-independent for *E-1*, they decrease when temperature increases for *E-2* (see Table 1). We tentatively attribute this temperature dependence of S_1 relaxation in *E-2* to the signature of a temperature-dependent population of various S_0 conformers having different S_1 vibrational relaxation pathways and kinetics. Further evidence of conformational heterogeneity of *E-2* is given below. Finally we note that at 50°C, both τ_2 and τ_3, hence the overall S_1 equilibration, are significantly faster in *E-2* than in *E-1*, which we attribute to the enlarged number of intramolecular degrees of freedom available upon linkage to the peptide, enabling faster vibrational energy dissipation.

Table 1. Time constants associated to each DAS as a function of temperature for compounds *E-1* and *E-2*. [a)]

	10°C		24°C		50°C	
	E-1	*E-2*	*E-1*	*E-2*	*E-1*	*E-2*
τ_1 (fs)	90	90	60	70	90	60
τ_2 (ps)	0.63	0.57	0.61	0.46	1.09	0.25
τ_3 (ps)	3.8	2.7	3.6	1.9	3.8	0.8
τ_4 (ps)	32	47 (50%)	28	33 (50%)	15	16 (65%)
τ_5 (ps)	--	330 (50%)	--	230 (50%)	--	94 (35%)

[a)] Time constants τ_1, τ_2, τ_3 are associated to vibrational and solvation relaxation kinetics in S_1, while τ_4 and τ_5 are attributed to S_1 population decay kinetics. The percentages in parenthesis are the relative weight of both decay components in the biexponential decay.

The longer-lived DAS have the same shapes as the spectra displayed in Figure 3C and 3H, and characterize the S_1 decay. For *E-1*, this decay is monoexponential, with a temperature-dependent time constant τ_4 ranging from 15 ps at 50°C to 32 ps at 10°C. This is the signature of an S_1 energy barrier to be overcome by thermal activation before effective decay to the ground state. Noticeably, for *E-2*, the S_1 decay is well fitted by a biexponential function with both time constants τ_4 and τ_5 depending on temperature. The faster time constant τ_4 is very similar to that of the bare photoswitch while τ_5 is systematically about 7 times slower. Hence the excited state lifetime is influenced by the peptide linkage and the biexponential decay is likely due to structural heterogeneity in the peptide, that is a distribution of (at least two) populations of conformers corresponding to different energy barrier heights on the S_1 PES. We note also that the relative weight for the fast decay component τ_4 increases at 50°C (see Table 1). This would indicate that higher temperature increases the population of a (less stable) S_0 conformer which would be characterized by a faster S_1 decay, as well as a faster S_1 equilibration (see above discussion on τ_2 and τ_3), as clearly illustrated by the comparison of the kinetic traces observed for various temperatures in Figure S2 in the ESI.

The temperature dependence of the S_1 lifetime of *E-1* (τ_4) *E-2* (τ_4 and τ_5, possibly characterizing the decay of two distinct sub-populations) are analyzed by Arrhenius plots (see Figure S3 and Table S1 in the ESI) seeking for an exponential dependence of the form: $1/\tau_{4,5} = A e^{-E_A/k_B T}$, with E_A the activation energy and A a pre-exponential factor. They reveal that (i) the activation energy for the free switch in solution (3.5 kcal·mol^{-1}, see ESI) is slightly lower than for the cross-linked peptide (by a factor 1.4 to 1.7 for the decay channels corresponding to τ_4 and τ_5, respectively), and (ii) the pre-exponential factors A appear significantly larger for compound 2. In particular, the τ_4 decay time constant is very similar for both compounds, although it corresponds to a larger activation energy (by a factor of ~1.4) for *E-2*. Under local equilibrium conditions where thermodynamic quantities are defined, the transition state theory relates A to the activation entropy[53, 54], which includes intramolecular as well as solvent (environment) contributions, the latter one being of major influence.[55-59]

Recently, the temperature dependence of the excited state lifetimes of a bilin chromophore covalently linked to a structurally heterogeneous phytochrome protein was analyzed similarly to

conclude that distinct protein conformers yielded significantly distinct prefactors A.[60] Here, on the one hand the peptide linkage increases the number of intramolecular degrees of freedom, but on the other hand the structural relaxation of the peptide is much slower than the photoisomerization and therefore restricts the accessible volume of the configurational space of the isomerizing subsystem. The detailed investigation of the change in activation entropy upon peptide linking is beyond the scope of the present paper. Instead, we focus below on the effect of the peptide linkage and peptide conformation on the S1 potential energy barrier height.

Computational Results

Excited State Pathways of *E*-1 in MeOH. The calculation of the absorption spectrum was performed at the CASPT2/MM level of theory. The optically bright state is found to be the first singlet excited state (S_1), with a S_0-S_1 excitation energy of 3.09 eV for the S_0 optimized geometry, in good agreement with the experimental value of 3.18 eV. Moreover, the electronic transition exhibits a high oscillator strength of *ca.* 1.0 and corresponds to a monoexcitation from a π orbital (centered on one phenyl ring and the photoisomerizable double bond) to its corresponding π* orbital, as illustrated in Figure 2D.

The MEP computed on S_1 from the Franck–Condon (FC) geometry first evidences an abrupt energy loss of *ca.* 10 kcal·mol^{-1} along the bond length alternation mode of the sp^2 carbon backbone, meaning that the stretching mode is activated, as is expected for such protonated Schiff bases.[7] Afterwards, a potential energy minimum is reached upon a very small torsion (*ca.* 2 degrees) around the isomerizing bond as illustrated in Figures 4A and S13 (see ESI).

The critical points are depicted, including the S_1 minimum and the S_1/S_0 conical intersection (CI). On the ground state, the internal conversion pathway back to the *E*-1 and the formation of *Z*-1 as photoproduct are shown.

A S_1 transition state (TS) is then located, corresponding to an energy barrier of *ca.* 3 kcal·mol^{-1} at the CASPT2 level of theory, which connects the S_1 minimum to the conical intersection with the ground state (S_1/S_0 CI). The corresponding reaction coordinate mainly implies torsion around the isomerizing double bond. The torsion angle is ϕ_{CCCH} = 30 degrees at the TS. After decay to the ground state, two paths are possible, which are reversion or photoisomerization (see Figure 4B). In the ground state, the *Z* photoisomer is predicted to be less stable than the *E* isomer (by 10.3 kcal·mol^{-1} at the CASPT2 level), as observed experimentally, with a S_0 energy barrier high enough to prevent thermal ground state isomerization at room temperature.[17]

Ground-State Dynamics and Characterization of *E*-2 and *Z*-2. The distance between the two sulfur atoms (SS distance) of the cysteine residues was analyzed as a measure of the switch end-to-end distance, which gives direct and crucial information about the effect of the switch linkage on the peptide structure. We first compare the average value of the SS distance along the MD simulations for the free peptide, *E*-2 and *Z*-2 in water. It was found to be 15.3 ± 2.2 Å, 13.7 ± 2.0 Å and 6.2 ± 1.7 Å respectively (see Figure 5A). Hence, we can conclude that the SS average distance of *E*-2 is in the range of the one found for the free peptide, and that the peptide secondary structure should be kept when linking the *E* isomer of the switch. Instead the SS average distance is reduced by *ca.* 7.5 Å in *Z*-2, that is upon photoisomerization, a value larger than the end-to-end distance change for azobenzene in similar applications.[61]
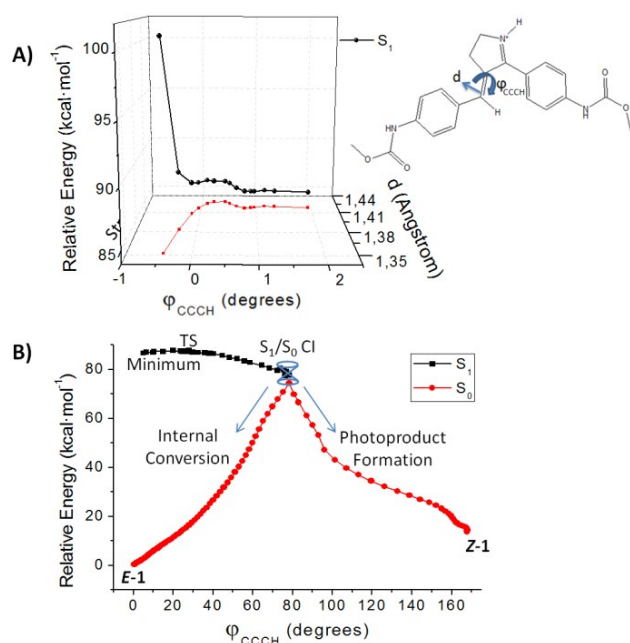

Figure 4. Overall MEP of *E*-1 in MeOH at the CASSCF level of theory: A) on the S_1 state from the FC structure to the S_1 minimum. The stretching and torsion modes are depicted. B) MEP from the excited transition state (TS) as a function of the torsional coordinate, ϕ_{CCCH}.
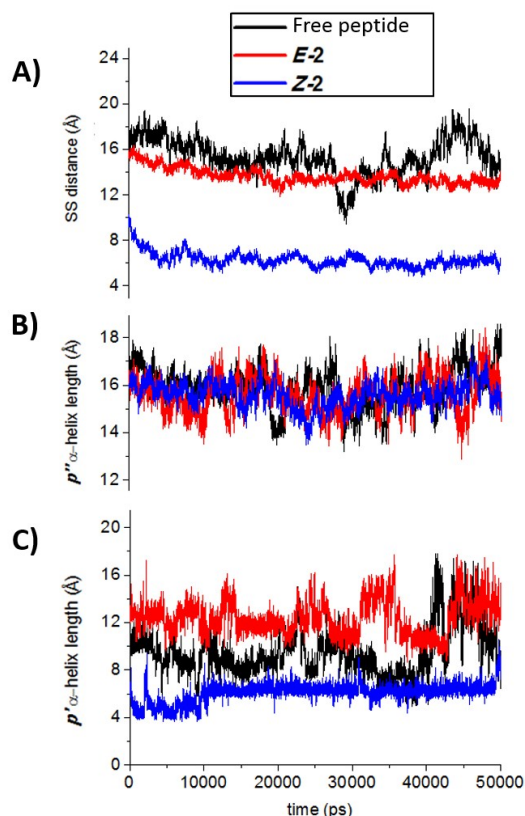
Figure 5. Peptide structure characterization. A) SS distance, B) *p''* and C) *p'* helix length along the MD simulation time for the free peptide (black line), *E*-2 (red line) and *Z*-2 (blue line).

Moreover, the length of the α-helix was analyzed for the three systems in order to understand the effect of the switch linkage and photoisomerization on the peptide secondary structure. We obtain average α-helix lengths of 25.4, 26.8 and 23.4 Å for the free peptide, *E*-2 and *Z*-2 respectively. First we note that the helicity percentage predicted by MD simulations for the free peptide (65%) is relatively high, as is expected for such a peptide where the high content of alanine residues is known to stabilize the α-helix content[31, 32]. In addition, the predicted length of the α-helix is larger in *E*-2 than in the free peptide indicating a stabilization of this secondary structure when the switch is attached. This observation is in line with the percentages of helical content found for the free peptide (65%) and *E*-2 (69%) and their CD spectra.[17] Interestingly, this is one of the few examples where the cross linking enhances the peptide helical content.[26, 62, 63]

Upon *E* to *Z* photoisomerization, the percentage of helical content is found to decrease slightly, as indicated both by the MD

simulations (*E*-2 (69%) and *Z*-2 (61%)) and the measured CD spectra (*E*-2 (79%) and *Z*-2 (60%)[17, 64]). This indicates that some aminoacids of *Z*-2 loose the helical arrangement. In order to further characterize the conformational change, we divided the peptide into two halves – *p'* from W1 to R14 (including the C4 switch linking site) and *p''* from C15 (the other linking site) to Q27, see Figure 1B – and calculated the α-helix length for each half. It was observed that the helix length of *p''* is almost invariant for the free peptide (15.9 Å), *E*-2 (15.6 Å) and *Z*-2 (15.8 Å) (see Figure 5B). Instead, the *p'* helix length is significantly different for the three models, namely 9.5, 11.3 and 7.9 Å for the free peptide, *E*-2 and *Z*-2 respectively (see Figure 5C). We conclude comparing the free peptide and *E*-2 that the switch attachment does not affect the *p''* helix half but does stabilize the α-helix in the *p'* half. Moreover, the photoisomerization affects almost exclusively the helical content of the *p'* helix half where the loss of helicity from *E*-2 to *Z*-2 is located.

Furthermore, this partial loss of helical content observed for *Z*-2 is mainly located in the region A13 to R18 (see coil, bend and turn events for these amino acids between α-helical regions in Figure 6). This structural modifications result in an α-hairpin secondary structure, as observed in seven out of ten *Z*-2 trajectories (see Figure 6 and movie in the ESI). The remaining three trajectories also exhibit a helix bending in the same region of the peptide, and a higher simulation time would possibly result in the formation of an α-hairpin structure also in these cases. Hence, the switch photoisomerization promotes a reversible peptide structural rearrangement, from α-helix to α-hairpin with a slight loss of helicity.

This reversible photo-conversion of the secondary structure predicted by the MD simulations agrees well and rationalizes the loss of helical content previously observed by circular dichroism spectroscopy on the same system[17] when forming *Z*-2. Moreover, the present MD results give detailed, atomistic-level insights into the peptide conformational change, which could not be revealed experimentally.

To further validate the MD simulation results we also computed the electronic absorption spectra of *E*-2 and *Z*-2 (see Methods) and compared them to the experimental data as shown in Figure 2. For *E*-2, the optically bright state is also S_1 and its electronic nature is the same as for *E*-1 (Figure 2D). The calculated S_0-S_1 excitation energies are around 380 and 370 nm for *E*-2 and *Z*-2 at the TD-DFT/MM level of theory (see ESI), which are in very good agreement (within less than 0.1 eV) with the experimental values. Moreover, the shapes of both simulated spectra are very similar to the experimental ones (see Figure 2B, C). Hence, we conclude that the present MD study yields a suitable description of the system in the ground state.
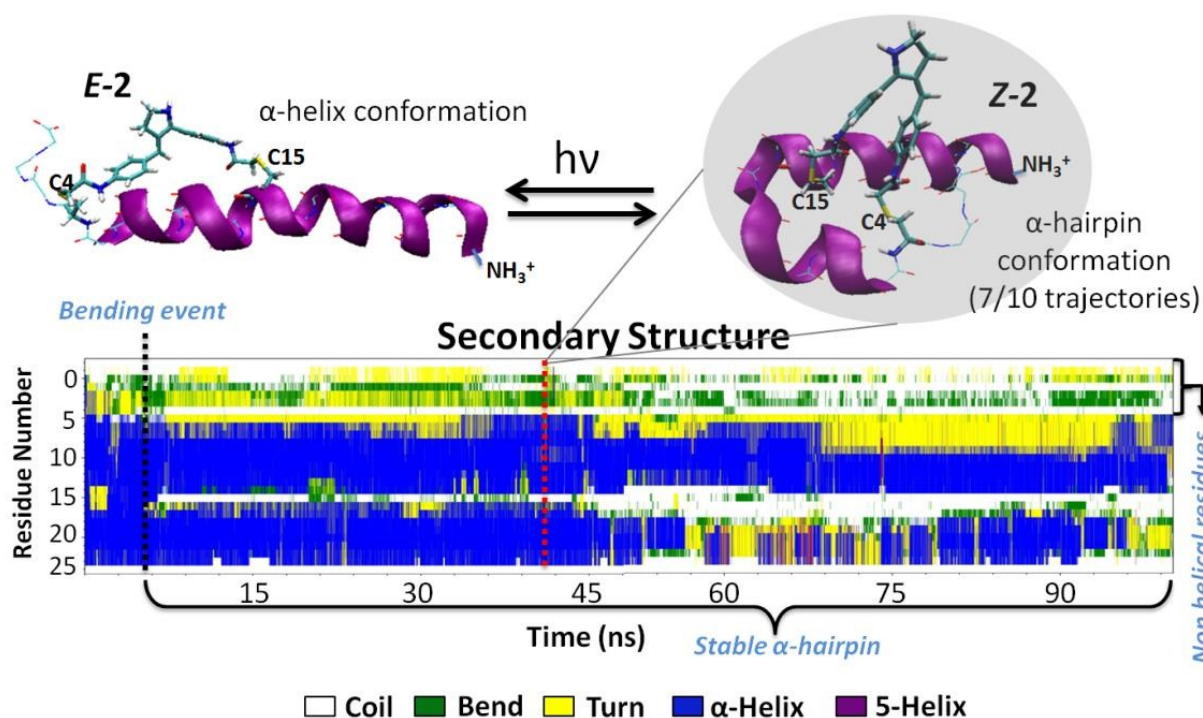
Figure 6. (Top) Snapshots of the MD simulations representative of the conformational change triggered by the photoisomerization. (Bottom) Time evolution of **Z-2** secondary structure using the DSSP (Define Secondary Structure of Proteins) method.[65, 66] Blue regions denote α-helical structures. At around 5.5 ns a bending event promotes the formation of a stable α-hairpin (see the white region around residue 15 splitting the blue region in two different sides). The first five residues are highly fluctuating and never shape into an α-helix.

Finally, beyond the above structural analysis in terms of average helical content, a cluster analysis (see ESI) of the MD trajectories of **E-2** evidences conformational heterogeneity, which is of central importance for the interpretation of the transient absorption data described above. In particular two distinct dominating conformations of the peptide are predicted, which differ mainly in their SS distance: 50% of the geometries have an SS average distance of 14.7 Å, while 18% corresponds to a shorter SS distance of 11.5 Å (Figure 7). Due to the peptide flexibility in water, several intermediate structures are predicted, each of them accounting for a proportion lower than 10%. We note here, that the experimentally observed S_1 decay is fitted by a biexponential decay which may actually also account for a continuous distribution of exponentially decaying functions with intermediate lifetimes, and therefore does not exclude a distribution of more than two conformers.
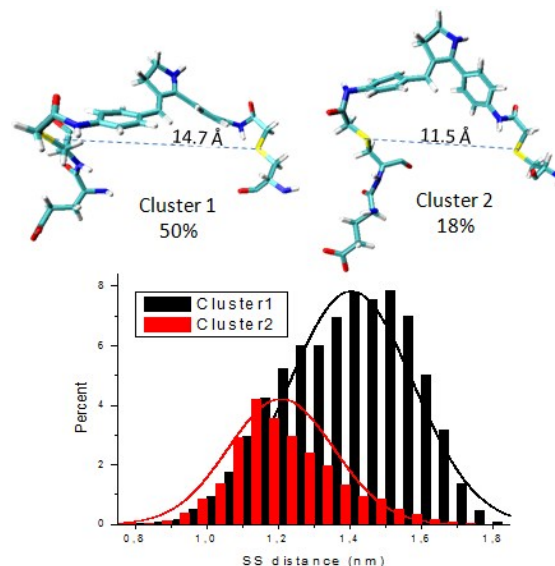

Figure 7. Histograms of the SS distance distributions of the two most relevant conformers of **E-2**, as extracted by cluster analysis along the MD trajectory. The total percentage of occurrences is shown.

Noticeably, this conformational flexibility is not induced by the attached switch, but is an inherent property of this peptide

sequence, as demonstrated by the clustering analysis of the free peptide, which shows almost the same results as for **E-2** (see ESI). Nevertheless, the two identified clusters cannot be distinguished spectroscopically, since their absorption spectra do overlap, as predicted at the CASPT2 level of theory (see Figure S8 in ESI for details).

Excited-State Dynamics and Pathways of E-2. In order to understand the effect of the peptide on the switch photoreactivity, the *E*-to-*Z* photoisomerization mechanism of the cross-linked peptide was investigated by calculating the excited-state pathway for a representative structure of each of the two clusters illustrated in Figure 7: two snapshots, named **E-2-C1** (from cluster 1) and **E-2-C2** (from cluster 2), were selected and optimized at the MP2/MM level to refine their FC geometry, followed by a calculation of the S_1 MEP for each conformer (see Methods).

Similarly to **E-1** in MeOH, after excitation to S_1, the bond length alternation due to stretching relaxation and a slight torsion of the double bond drive the system to a potential energy minimum (see Figure S10 in the ESI). To find the transition states (TS) connecting the S_1 PES minimum to the CI, the PES is mapped by a double scan around ϕ_{CCCH} and ϕ_{CCCC}, which are the most relevant coordinates to describe the torsion around the central isomerizing bond in retinal-like molecular switches.[67] For **E-2-C1** a high energy region is found to connect the S_1 minimum and the CI via a saddle point that we identify as the TS, characterized by ϕ_{CCCH} = 45º and ϕ_{CCCC} = 35º (Figure 8). The energy barrier calculated at the CASPT2 level is ≈ 13 kcal·mol^{-1}. From the TS geometry, a MEP is computed toward the S_1 PES minimum and toward the CI. The rotation around the double bond from the S_1 minimum in the opposite sense (*i.e.* counterclockwise) was also evaluated. A similar CASPT2 energy barrier of ≈ 14 kcal·mol^{-1} is found indicating that both clockwise and counterclockwise paths are almost equivalent.
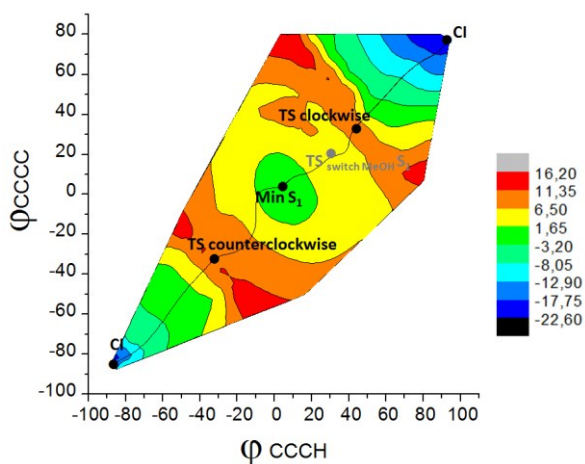

Figure 8. Energy map as a result of the double scan around ϕ_{CCCH} and ϕ_{CCCC} for **E-2-C1**. The critical points are depicted: TS, S_1 minimum, S_1/S_0 conical intersections (CI) and, for geometrical comparison, the TS of the switch in MeOH. The MEP connecting the TS with the minimum and the CI is shown in black.

Applying the same methodology, the TS geometry for **E-2-C2** was identified at ϕ_{CCCH} = 20º and ϕ_{CCCC} = 40º, corresponding to an S_1 energy barrier of ≈ 5 kcal·mol^{-1} at the CASPT2 level of theory. Again, the MEPs from the TS to the S_1 minimum and the CI are computed.

We can therefore conclude that both conformers minimize the energy from the TS along the torsion coordinate until reaching the S_1/S_0 CI. From there, the system decays to the ground state completing the photoisomerization or recovering the starting isomer. These two possible paths have been calculated for both conformers, **E-2-C1** and **E-2-C2** (Figure S11 in the ESI).

In the case of **E-2-C1**, non-adiabatic molecular dynamic trajectories were performed on S_1, in order to give insights about the photoisomerization mechanism. Because of the high S_1 energy barrier and the rather long excited-state lifetime (of the order of hundreds of ps), a dynamical study describing the whole process is computationally unfeasible. Hence, we calculated trajectories with zero initial kinetic energy (*i*) from the Franck–Condon region toward the S_1 minimum, (*ii*) from the TS toward the S_1 minimum and (*iii*) from the TS to the ground state, either isomerizing or reverting back to the initial switch conformation. This allowed for a direct comparison with the calculated MEP. The results are illustrated in Figure 9 and show that the overall trajectory (from the FC geometry to the formation of the photoisomer) describes the relation between C=C stretching and torsion in agreement with the calculated MEP. Especially, a complete decoupling between the two coordinates is never observed. Instead, in the excited state the C=C bond lengthening is firstly observed coupled to a slight torsion. Once the carbon-carbon bond becomes completely a single bond, the hydrogen-out-of-plane mode drives the reaction towards the intersection with the ground state, finally allowing to form the *Z* isomer while recovering the double bond character of the C=C central bond.[67] Noticeably, along these excited state trajectories and as also found through the MEP, the structural changes of the peptide moiety are limited to subtle rearrangements (*ca.* 2.0 Å) of the amino acids in the vicinity of the switch, and in the peptide region which is going to bend, especially W1, A6, A7, A8, E10, A11, A12, A13, R14 and C15. Indeed, these amino acids form a sort of pocket around the switch and their move favors the geometrical displacements required to afford the *E*-to-*Z* isomerization (see Figure S12 in ESI). The actual, larger scale peptide bending of the A13 to R18 segment, and hairpin formation occur only after the decay to the ground state, on a much longer time scale.
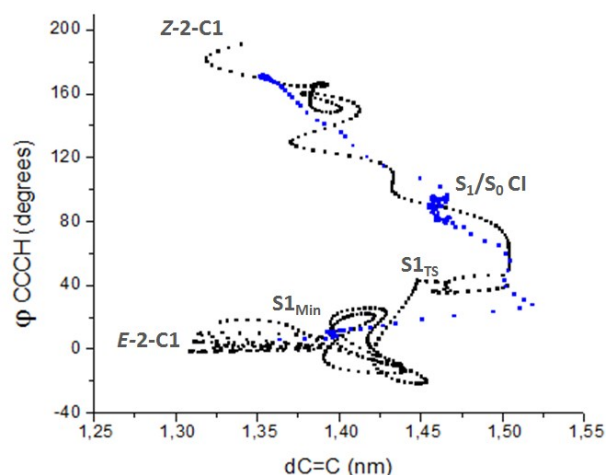
Figure 9. Non-adiabatic MD simulation (black) and MEP (blue) of **2-C1** E-to-Z photoisomerization, as a function of the two most relevant coordinates: stretching and torsion around the central C=C bond.

Summarizing, Figure 10 shows all investigated photoisomerization pathways as a function of the central C=C bond torsion. **E-1** and **E-2-C2** appear to have similar S_1 topologies, characterized by a transition state located between 20 and 30 degrees of torsion and a S_1 energy barrier between 3 and 5 kcal·mol^{-1}. On the other hand, **E-2-C1** shows a transition state above 40 degrees of torsion, associated to a higher S_1 energy barrier (*ca.* 13 kcal·mol^{-1}). Moreover, the S_1/S_0 intersection region is lower in energy (17 kcal·mol^{-1} at the CASPT2 level) and located at *ca.* 15 degrees higher torsion in the case of **E-2-C1**, when compared to **E-2-C2** and **E-1.**
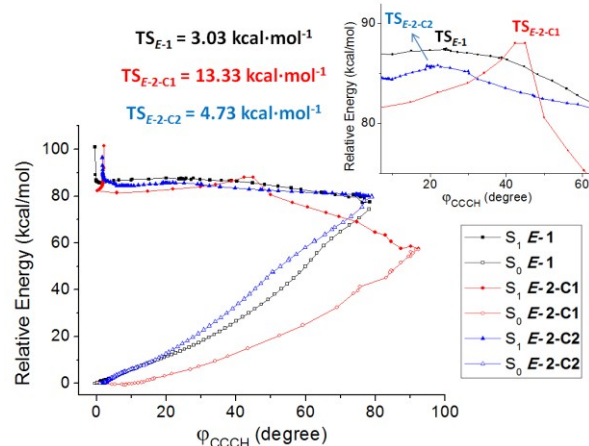

Figure 10. CASSCF excited state pathways of **E-2-C1** (red lines), **E-2-C2** (blue lines) and **E-1** (black lines), as a function of the torsion around the photoisomerizable C=C bond. The inset shows the position and CASPT2 corrected energy barrier for each S_1 transition state (TS).

Discussion

The overall mechanism from photon absorption to formation of the photoisomer can be summarized by three main steps: vibrational relaxation from the Franck–Condon region to the S_1 minimum; excited state population decay to the electronic ground state; conformational changes involving switch relaxation and peptide secondary structure reorganization.

The non-exponential S_1 vibrational and solvation dynamics evidenced by TAS and documented with three time scales spanning from sub-100 fs to a few ps is fully rationalized by the MEP calculations and non-adiabatic molecular dynamics. Indeed the latter evidence the excitation and early relaxation out of the FC region along (high-frequency) stretching modes which cause partial bond length alternation in the chromophore. This confers, at least partially, a single bond character to the central isomerizing carbon-carbon bond and enables the subsequent contribution of lower frequency modes to the reaction coordinate, and in particular the slower torsion motion around the isomerizing C-C bond. As a matter of fact, for all models the corresponding ϕ_{CCCC} torsion angle (see Figure 1A) is twisted at the S_1 minimum (see below). Also the reorganization of the polar solvent (MeOH in compound **1** or water in compound **2**) and of the peptide (compound **2** only) around the chromophore is expected to occur on the sub-ps to ps time scale, given the charge transfer character of the S_1 electronic state, described by partial migration of the positive charge from the five-membered ring to the phenyl moiety (see Figure 2D).

The main difference observed by TAS between **E-1** and **E-2** is in the S_1 population decay kinetics, being monoexponential (τ4) for **E-1** and biexponential (τ4 and τ5) for **E-2** (see Figure 3). The QM/MM study of **E-1** predicts a 3 kcal·mol^{-1} S_1 energy barrier between the S_1 minimum and the CI, which is in line with the thermally activated S_1 decay observed experimentally. For **E-2**, the MD simulations predict structural heterogeneity with, in particular, two main conformers of **E-2**, **C1** and **C2**. The QM/MM calculations conclude that both conformers influence differently the S_1 PES topologies and in particular the S_1 energy barriers. The 5 and 13 kcal·mol^{-1} energy barriers predicted for **C2** and **C1** respectively (see Figures 8 and 10) should be considered as upper boundaries for the S_1 energy barriers since they result from the 2D exploration of a multidimensional PES. Still, identification of different conformers exhibiting different S_1 energy barriers is in agreement with the experimental observation of a temperature-dependent biexponential S_1 decay, indicating the presence of (at least) two populations undergoing thermally activated population decay along distinct pathways. In addition, the predicted similarity of the PES topologies of compounds **E-1** in MeOH and **E-2-C2** in water is in line with the similar values observed for τ4 in both compounds, while the expected properties of **E-2-C1** are in line with the larger value of τ5.

We now discuss the mechanism by which the peptide linkage alters the PES topology and therefore the photoreactivity of the switch. First, we note that although both **E-2-C1** and **E-2-C2** are characterized by a significantly distinct average SS-distance (see Figure 7) and S_1 energy barrier (see Figure 10), the degrees of freedom primarily involved in the photoswitch reaction coordinate have ground state values very similar in both conformers and not either very different from **E-1** (see table S4 in the ESI). Interestingly, only in **E-2-C2** the ϕ_{CCCC} pretwist in increased to about 11°, but this

ARTICLE

is apparently not affecting significantly the S_1 properties of **E-2-C2** with respect to **E-1**. This is in contrast to the photophysics of retinal proteins where 10 to 15° initial pretwist of the izomerizing bond is argued to be of major influence on the retinal photoreactivity (see below). We conclude that in the present case of thermal-activation in S_1, the initial FC geometry (and peptide constraint) is less critical at influencing the photoreactivity than in a nearly ballistic (sub-picosecond) reaction as observed in retinal proteins.

Instead, the comparison between the **E-2-C1** and **E-2-C2** geometries at the S_1 minimum and TS suggests a structural explanation for their difference in the S_1 energy barriers. At the minimum of S_1, the bond length alternation is not completed for both conformers (*i.e.* the isomerizing bond still has a partial double bond character). Therefore, some energy is required in order to proceed with the isomerization process which requires torsion around that bond. In the case of **E-2-C1** however, the bond length alternation and the ϕ_{CCCC} torsion are even less advanced than for **E-2-C2** (see details in Table S4 in the ESI) thus explaining by electronic structure the presence of an enhanced excited state barrier in **E-2-C1**. This is also in line with the TS being characterized by (*i*) a larger value of the hydrogen-out-of-plane and (*ii*) a larger pyramidalization of the PSB nitrogen atom for **E-2-C1**, than for **E-2-C2** (see details in table S4 in the ESI). The structural parameters described for **E-2-C2** are instead closer to those of **E-1**, which has an even lower energy barriers since its bond length alternation at the S_1 minimum is almost complete.

Also consistent with the structural differences described above, the excited state charge transfer character of the TS state is almost complete for **E-2-C1**, while only half of the charge migrated in **E-2-C2** or in **E-1** (see details in table S4 in the SI). Moreover, the charge transfer character is found to be related to the surrounding environment of the molecular switch. Indeed, a deprotonated C-terminus is expected considering the acidic experimental conditions (pH = 4.3) compared to the pKa value of the W residue (2.46). We observe that the C-terminus tends to adopt two main arrangements along the trajectories, either placing the COO^- group next to the switch six-membered ring directly bound to the photoisomerizable C=C bond, or exposing the COO^- group to water. The former case enhances positive charge translocation along the switch and corresponds to **E-2-C1** (see Figure S12 in ESI), while the latter case does not favor a notable charge transfer and corresponds to **E-2-C2**.

Hence we conclude that both, the electrostatic embedding and the mechanical force exerted at both ends of the switch by the covalently-linked peptide, are responsible of the different S_1 energy barriers.

It is noteworthy to compare such a mechanistic and dynamic scenario (see Figure 9 and 10) with previous studies performed on similar PSBs (especially retinal) in solution or as rhodopsin chromophore: in all cases the photochemical pathway involves charge translocation, already in the FC region, which triggers bond length alternation of the conjugated backbone followed by torsion and isomerization through a CI. In spite of a similar mechanistic description, the reaction kinetics can be largely different, depending on the environment. Indeed, a sub-ps photoisomerization is observed in retinal proteins,[68] where the opsin pocket induces (*i*) a pre-twisting of the isomerizing bond already in the ground state due to steric interaction [69] and (*ii*) an

electrostatic field increasing the efficiency of the charge transfer driving the process[70]. Instead, the retinal PSB in solution behaves differently, since in this case the homogeneous environment does not induce any specific pre-twist nor enhanced charge translocation along the backbone. In the latter case, a planar S_1 region or even a small energy barrier[71] slows down the isomerization process, reaching the ps time scale, as observed in **1**. On the other hand, in **2** the S_1 energy barrier can be even higher than in **1**, due to the different constraints imposed by the peptide attachment, that induce electrostatic interactions and forces at both sides of the switch. Moreover, the flexibility of the peptide creates different possible charge arrangements around the molecular switch (to a large extent sequence dependent).

Finally, when focusing the attention on the peptide, the extensive MD study of the free peptide, **E-2** (10 trajectories of 50 ns) and **Z-2** (10 trajectories of 100 ns) served to find out the switch linkage and photoisomerization effects on the peptide secondary structure. As the SS distance of the free peptide and **E-2** along the simulation time are very similar (see Figure 5A), we do not expect a large secondary structure change upon the switch linkage. Upon photoisomerization, a reversible secondary structural change from an α-helix (**E-2**) to an α-hairpin (**Z-2**). Moreover, the MD analysis of **E-2** allowed us to evince its intrinsic structural heterogeneity, thus rationalizing the observed photodynamics behavior.

Conclusions

Combining state-of-the-art transient absorption spectroscopy and multiscale simulations, we were able to reveal the dynamical and mechanistic differences between the photoisomerization of a retinal-like, synthetic molecular switch in solution or cross-linked to a peptide. In the present case, we found that the polypeptide linkage modifies the excited state topology and therefore the reactivity of the switch, in a way that depends on the heterogeneous ground state peptide conformation. Especially, the excited state decay time increases up to one order of magnitude (at room temperature) when cross-linked to the polypeptide, nevertheless always enabling a successful isomerization, as proved by the photoisomerization quantum yield previously measured for these two compounds.[17] This is rationalized by evidencing, both experimentally and theoretically, the influence of the peptide linkage on the excited-state energy barrier. It has been concluded that different conformers, in particular **E-2-C1** and **E-2-C2**, exhibit different electronic and structural properties along their pathway from the FC region back to the ground state. Particularly, **E-2-C2** behaves similarly to **E-1**: the central C=C bond is significantly elongated after S_1 vibrational relaxation, and the transition state is characterized by a *ca.* 25º torsion and an energy barrier below 5 kcal·mol^{-1}. Whereas, for **E-2-C1** the C=C bond has a significant character of double bond leading to a higher energy barrier and a transition state retarded along the torsion coordinate (*ca.* 45º).

This work can be seen as a bottom-up approach for the investigation of the influence of the surrounding environment of a molecular switch on its photoreactivity where, starting from the bare synthetic chromophore, we have considered the effect of its linking to a peptide. This is a central issue (exemplified *e.g.* by the influence of the opsin pocket on the retinal photochemistry) which

is to be carefully explored in the view of designing synthetic chromophores for the efficient photoswitching of molecular functions. In the specific case explored here, we show that combined transient absorption spectroscopy and extensive modeling are efficient tools to reveal the mechanism and ability of a retinal-like molecular switch to efficiently convert an α-helix into an α-hairpin in a process spanning from photon absorption to macromolecular conformational change on time scales from the fs to the μs time range.

Acknowledgements

References

1. T. R. Kelly and Editor, *Molecular Machines. [In: Top. Curr. Chem., 2005; 262]*, Springer, 2005.
2. V. Balzani, *ChemPhysChem*, 2009, **10**, 21.
3. B. L. Feringa, W. R. Browne and Editors, *Molecular Switches, Volume 2: Second, Completely Revised and Enlarged Edition*, Wiley-VCH Verlag GmbH & Co. KGaA, 2011.
4. C. Garcia-Iriepa, M. Marazzi, L. M. Frutos and D. Sampedro, *RSC Adv.*, 2013, **3**, 6241-6266.
5. W. Szymanski, J. M. Beierle, H. A. V. Kistemaker, W. A. Velema and B. L. Feringa, *Chem. Rev. (Washington, DC, U. S.)*, 2013, **113**, 6114-6178.
6. I. Willner and B. Willner, 2001.
7. S. Gozem, F. Melaccio, H. L. Luk, S. Rinaldi and M. Olivucci, *Chem. Soc. Rev.*, 2014, **43**, 4019-4036.
8. C. Renner and L. Moroder, *ChemBioChem*, 2006, **7**, 868-878.
9. A. A. Beharry and G. A. Woolley, *Neuromethods*, 2011, **55**, 171-184.
10. H. Janovjak and E. Y. Isacoff, *Neuromethods*, 2011, **55**, 233-266.
11. M. Erdelyi, A. Karlen and A. Gogoll, *Chem. - Eur. J.*, 2006, **12**, 403-412.
12. M. Erdelyi, M. Varedian, C. Skoeld, I. B. Niklasson, J. Nurbo, A. Persson, J. Bergquist and A. Gogoll, *Org. Biomol. Chem.*, 2008, **6**, 4356-4373.
13. N. J. V. Lindgren, M. Varedian and A. Gogoll, *Chem. - Eur. J.*, 2009, **15**, 501-505.
14. T. Cordes, C. Elsner, T. T. Herzog, C. Hoppmann, T. Schadendorf, W. Summerer, K. Rueck-Braun and W. Zinth, *Chem. Phys.*, 2009, **358**, 103-110.
15. N. Regner, T. T. Herzog, K. Haiser, C. Hoppmann, M. Beyermann, J. Sauermann, M. Engelhard, T. Cordes, K. Rueck-Braun and W. Zinth, *J. Phys. Chem. B*, 2012, **116**, 4181-4191.
16. T. Andruniow, S. Fantacci, F. De Angelis, N. Ferre and M. Olivucci, *Angew. Chem., Int. Ed.*, 2005, **44**, 6077-6081.
17. M. Blanco-Lomas, S. Samanta, P. J. Campos, G. A. Woolley and D. Sampedro, *J. Am. Chem. Soc.*, 2012, **134**, 6960-6963.
18. A. Sinicropi, C. Bernini, R. Basosi and M. Olivucci, *Photochem. Photobiol. Sci.*, 2009, **8**, 1639-1649.
19. J. A. McCammon and P. G. Wolynes, *Curr. Opin. Struct. Biol.*, 2002, **12**, 143-145.
20. C. D. Snow, H. Nguyen, V. S. Pande and M. Gruebele, *Nature (London, U. K.)*, 2002, **420**, 102-106.
21. R. Schweitzer-Stenner and Editor, *Protein and Peptide Folding, Misfolding, and Non-Folding*, John Wiley & Sons, Inc., 2012.
22. P. H. Nguyen, Y. Mu and G. Stock, *Proteins: Struct., Funct., Bioinf.*, 2005, **60**, 485-494.
23. P. H. Nguyen, H. Staudt, J. Wachtveitl and G. Stock, *J. Phys. Chem. B*, 2011, **115**, 13084-13092.
24. G. A. Woolley, *Acc. Chem. Res.*, 2005, **38**, 486-493.
25. D. G. Flint, J. R. Kumita, O. S. Smart and G. A. Woolley, *Chem. Biol.*, 2002, **9**, 391-397.
26. A. M. Ali and G. A. Woolley, *Org. Biomol. Chem.*, 2013, **11**, 5325-5331.
27. J. Bredenbeck, J. Helbing, J. R. Kumita, G. A. Woolley and P. Hamm, *Proc. Natl. Acad. Sci. U. S. A.*, 2005, **102**, 2379-2384.
28. L. Rivado-Casas, M. Blanco-Lomas, P. J. Campos and D. Sampedro, *Tetrahedron*, 2011, **67**, 7570-7574.
29. D. Sampedro, A. Migani, A. Pepi, E. Busi, R. Basosi, L. Latterini, F. Elisei, S. Fusi, F. Ponticelli, V. Zanirato and M. Olivucci, *J. Am. Chem. Soc.*, 2004, **126**, 9349-9359.
30. B. H. Zimm and J. K. Bragg, *J. Chem. Phys.*, 1959, **31**, 526-535.
31. S. Marqusee and R. L. Baldwin, *Proc. Natl. Acad. Sci. U. S. A.*, 1987, **84**, 8898-8902.
32. S. Marqusee, V. H. Robbins and R. L. Baldwin, *Proc. Natl. Acad. Sci. U. S. A.*, 1989, **86**, 5286-5290.
33. S. Padmanabhan, E. J. York, L. Gera, J. M. Stewart and R. L. Baldwin, *Biochemistry*, 1994, **33**, 8604-8609.
34. M. Volk, Y. Kholodenko, H. S. M. Lu, E. A. Gooding, W. F. DeGrado and R. M. Hochstrasser, *J. Phys. Chem. B*, 1997, **101**, 8607-8616.
35. L. Milanesi, J. P. Waltho, C. A. Hunter, D. J. Shaw, G. S. Beddard, G. D. Reid, S. Dev and M. Volk, *Proc. Natl. Acad. Sci. U. S. A.*, 2012, **109**, 19563-19568, S19563/19561-S19563/19529.
36. P. Hamm, M. Zurek, T. Roeschinger, H. Patzelt, D. Oesterhelt and W. Zinth, *Chem. Phys. Lett.*, 1996, **263**, 613-621.
37. C. Punwong, J. Owens and T. J. Martinez, *J. Phys. Chem. B*, 2015, **119**, 704-714.
38. X. Li, L. W. Chung and K. Morokuma, *J. Chem. Theory Comput.*, 2011, **7**, 2694-2698.
39. K. Bravaya, A. Bochenkova, A. Granovsky and A. Nemukhin, *J. Am. Chem. Soc.*, 2007, **129**, 13035-13042.
40. O. Bismuth, N. Friedman, M. Sheves and S. Ruhman, *Chem. Phys.*, 2007, **341**, 267-275.
41. J. Briand, O. Braem, J. Rehault, J. Leonard, A. Cannizzo, M. Chergui, V. Zanirato, M. Olivucci, J. Helbing and S. Haacke, *Phys. Chem. Chem. Phys.*, 2010, **12**, 3178-3187.

ARTICLE

Journal Name

42. V. Hornak, R. Abel, A. Okur, B. Strockbine, A. Roitberg and C. Simmerling, *Proteins: Struct., Funct., Bioinf.*, 2006, **65**, 712-725.

43. J. Wang, R. M. Wolf, J. W. Caldwell, P. A. Kollman and D. A. Case, *J. Comput. Chem.*, 2004, **25**, 1157-1174.

44. J. Finley, P.-A. Malmqvist, B. O. Roos and L. Serrano-Andres, *Chem. Phys. Lett.*, 1998, **288**, 299-306.

45. J. C. Tully, *J. Chem. Phys.*, 1990, **93**, 1061-1071.

46. see http://www.gromacs.org/.

47. R. Salomon-Ferrer, D. A. Case and R. C. Walker, *Wiley Interdiscip. Rev.: Comput. Mol. Sci.*, 2013, **3**, 198-210.

48. F. Aquilante, L. De Vico, N. Ferre, G. Ghigo, P.-a. Malmqvist, P. Neogrady, T. B. Pedersen, M. Pitonak, M. Reiher, B. O. Roos, L. Serrano-Andres, M. Urban, V. Veryazov and R. Lindh, *J. Comput. Chem.*, 2010, **31**, 224-247.

49. J. W. Ponder and F. M. Richards, *J. Comput. Chem.*, 1987, **8**, 1016-1024.

50. Y. Zhao and D. G. Truhlar, *Theor. Chem. Acc.*, 2008, **120**, 215-241.

51. M. J. T. Frisch, G. W.;Schlegel, H. B.; Scuseria, G. E.; Robb, M. A.; Cheeseman, J. R.; Scalmani, G.; Barone, V.; et al. , *Gaussian 09 revision B.01; Gaussian, Inc.: Wallingford, CT* 2009.

52. T. Vreven, K. S. Byun, I. Komaromi, S. Dapprich, J. A. Montgomery, Jr., K. Morokuma and M. J. Frisch, *J. Chem. Theory Comput.*, 2006, **2**, 815-826.

53. E. V. D. Anslyn, Dennis A., *Transition State Theory and Related Topics. In Modern Physical Organic Chemistry*, University Science Books, 2006.

54. K. J. J. Laidler, *Journal of physical chemistry (1952)*, 1983, **87**, 2657-2664.

55. J. Dokic, M. Gothe, J. Wirth, M. V. Peters, J. Schwarz, S. Hecht and P. Saalfrank, *J. Phys. Chem. A*, 2009, **113**, 6763-6773.

56. S. A. Kovalenko and A. L. Dobryakov, *Chem. Phys. Lett.*, 2013, **570**, 56-60.

57. D. A. Harris, M. B. Orozco and R. J. Sension, *J. Phys. Chem. A*, 2006, **110**, 9325-9333.

58. F. X. Vazquez, S. Talapatra, R. J. Sension and E. Geva, *J. Phys. Chem. B*, 2014, **118**, 7869-7877.

59. M. Strajbl, Y. Y. Sham, J. Villa, Z. T. Chu and A. Warshel, *J. Phys. Chem. B*, 2000, **104**, 4578-4584.

60. P. W. Kim, N. C. Rockwell, S. S. Martin, J. C. Lagarias and D. S. Larsen, *Biochemistry*, 2014, **53**, 2818-2826.

61. D. C. Burns, D. G. Flint, J. R. Kumita, H. J. Feldman, L. Serrano, Z. Zhang, O. S. Smart and G. A. Woolley, *Biochemistry*, 2004, **43**, 15329-15338.

62. J. R. Kumita, O. S. Smart and G. A. Woolley, *Proc. Natl. Acad. Sci. U. S. A.*, 2000, **97**, 3803-3808.

63. F. Zhang, O. Sadovski, S. J. Xin and G. A. Woolley, *J. Am. Chem. Soc.*, 2007, **129**, 14154-14155.

64. E. Lacroix, A. R. Viguera and L. Serrano, *J. Mol. Biol.*, 1998, **284**, 173-191.

65. W. Kabsch and C. Sander, *Biopolymers*, 1983, **22**, 2577-2637.

66. C. A. F. Andersen, A. G. Palmer, S. Brunak and B. Rost, *Structure (Cambridge, MA, U. S.)*, 2002, **10**, 175-184.

67. I. Schapiro, M. N. Ryazantsev, L. M. Frutos, N. Ferre, R. Lindh and M. Olivucci, *J. Am. Chem. Soc.*, 2011, **133**, 3354-3364.

68. D. Polli, P. Altoe, O. Weingart, K. M. Spillane, C. Manzoni, D. Brida, G. Tomasello, G. Orlandi, P. Kukura, R. A. Mathies, M. Garavelli and G. Cerullo, *Nature (London, U. K.)*, 2010, **467**, 440-443.

69. L. M. Frutos, T. Andruniow, F. Santoro, N. Ferre and M. Olivucci, *Proc. Natl. Acad. Sci. U. S. A.*, 2007, **104**, 7764-7769.

70. K. Welke, J. S. Fraehmcke, H. C. Watanabe, P. Hegemann and M. Elstner, *J. Phys. Chem. B*, 2011, **115**, 15119-15128.

71. O. Valsson and C. Filippi, *J. Chem. Theory Comput.*, 2010, **6**, 1275-1292.